Research Article | Vol. 13, No. 2 / 1 Feb 2022 / Biomedical Optics Express 744
Biomedical Optics EXPRESS

Pyrometry with flexible infrared fibers for temperature-controlled laser surgery

ALEXANDER S. NOVIKOV,[1,2,*] ISKANDER USENOV,[1,2] DAWID SCHWEDA,[1] PHILIPP CAFFIER,[3] BJÖRN LIMMER,[4] VIACHESLAV ARTYUSHENKO,[2] AND HANS J. EICHLER[1]

[1]*Technische Universität Berlin, Straße des 17. Juni 135, 10623 Berlin, Germany*
[2]*art photonics GmbH, Rudower Chaussee 46, 12489 Berlin, Germany*
[3]*Department of Audiology and Phoniatrics, Charité - Universitätsmedizin Berlin, Charitéplatz 1, 10117 Berlin, Germany*
[4]*Limmer Laser GmbH, Schwarzschildstraße 1, 12489 Berlin, Germany*
[*]*an@artphotonics.de*

Abstract: Pyrometry is widely used in science, medicine, and industry to measure the surface temperature of objects in a non-contact way. IR fibers are an ideal solution for the flexible delivery of thermal radiation emitted from objects inside a complex structure like internal organs inside the human body. Silver halide polycrystalline infrared fibers (PIR) are transparent in a spectral range of 3 – 18 µm, matching perfectly with the spectra of black body radiation for temperatures ranging from 20°C to 200°C. These fibers are non-toxic and allow small bending radii. They could become critical components in pyrometric systems for temperature-controlled laser surgeries. Here we discuss the ability of the PIR fibers for simultaneous laser power delivery and real-time temperature monitoring in laser surgery applications and demonstrate two different setups for this purpose.

1. Introduction

1.1. Infrared thermometry

Objects with non-zero temperature continuously emit electromagnetic radiation that can be approximated as black-body radiation described by Planck law. Stefan-Boltzmann law describes the total emitted power j, proportional to the 4th power of the body's absolute temperature. Real surfaces emit less energy than a black body. They are known as gray bodies characterized by emissivity ε. In this case, the Stefan-Boltzmann law is modified to:

$$j = \varepsilon\sigma T^4, \tag{1}$$

where σ is the Stefan-Boltzmann constant, and ε is the emitting surface's emissivity at a fixed wavelength λ and temperature T. For a perfect black body, emissivity is equal to 1: $\varepsilon = 1$; for real materials, it is less than 1: $\varepsilon<1$. Numerical emissivity values of different human tissues are given in [1] and [2]. The emissivity of many biological tissues is about 0.9.

Absolute black body temperature can be related to the peak of the spectral radiance described by Wien displacement law and is inversely proportional to the body's absolute temperature. Manufacturers use this dominant wavelength to design thermal imaging sensors reaching the best match for the range of temperatures being measured [3]. Infrared (IR) thermometry relies on black-body radiation in the wavelength range from 5 to 14 μm corresponding to peak temperatures from 300 °C to −65 °C. That limits the system to measure only the surface temperature, so information about tissues' internal temperature cannot be provided [4]. Results also depend on the object's emissivity and distance-to-spot size ratio [5]. This technology is fast, passive, non-invasive, and can map body temperature. In the current COVID-19 pandemic, its ability to detect

#442024 https://doi.org/10.1364/BOE.442024
Journal © 2022 Received 6 Sep 2021; revised 5 Jan 2022; accepted 6 Jan 2022; published 14 Jan 2022

Biomedical Optics EXPRESS

fever is being exploited for mass screening worldwide [6]. It was successfully used to detect breast cancer, peripheral vascular disorders, diabetic neuropathy, and various other problems in many medical disciplines, e.g., gynecology, kidney transplantation, dermatology, brain imaging, and cardiovascular surgery. IR thermography can provide real-time, high-resolution thermographic images [7]. Devices based on IR thermometry are known as pyrometers and are used to measure the surface's temperature in a non-contact way. They consist of a detector and an optical system, which focuses the thermal radiation onto the detector.

The temperature control via IR thermography can be utilized during laser surgery operations. The absorption of laser radiation depends on tissue type, thickness, and state of hydration. Therefore, it is challenging to control the parameters and conditions needed to obtain good results. One of the most critical parameters is the heated spot temperature because slight overheating may lead to severe thermal damage to the tissues. At the same time, a low temperature may lead to an insufficient result [8].

Here we discuss the ability of the silver halide polycrystalline infrared (PIR) fibers for real-time temperature monitoring and laser power delivery at the same time for laser surgery applications. Two different designs were tested for a flexible laser delivery with temperature control. The first one utilizes one fiber to deliver laser power and the other fiber to collect IR radiation and measure a temperature. The second design is a common free space system where the same PIR cable is used for laser power delivery and IR radiation collection. In both cases, a simple calibration method is used with a commercially available pyrometer and the classical Stefan-Boltzmann law.

1.2. Optical fibers for transmission of thermal radiation and pyrometry

In order to increase the usability and flexibility of the laser surgery device, special fibers can be used to deliver the laser radiation and simultaneously collect thermal radiation from the heated spot [9]. For the mid-IR spectral range, various optical fibers are commercially available, e.g., chalcogenide IR (CIR), polycrystalline IR (PIR), hollow-core fibers (hollow waveguides) [10,11]. The fused silica fibers can also be used for pyrometry, but they have a limited mid-IR transmission [12]. PIR fibers made from solid solutions of silver halides ($AgCl_xBr_{1-x}$) have high transparency over a vast spectral range in the mid-IR region, low losses for 10.6 μm (the operating wavelength of a widely used CO_2 laser), insoluble in water, biocompatible, non-toxic, and very flexible [13,14]. In particular, PIR fibers have good transmission properties in a spectral range of 3 – 18 μm, which corresponds to a wavelength of heat radiation in a temperature range of about −100 °C to 450 °C. The most important temperature range in medical applications is from 30 °C to 300 °C, i.e., from body temperature to carbonization point and vaporization of the tissue. The transmission region of such fibers is matched almost perfectly with the spectra of black body radiation for temperatures ranging from 20°C to 200°C (Fig. 1), making them perfect candidates for implementing a noninvasive flexible temperature control, especially during surgical operations.

Moreover, since such fibers can also deliver laser radiation, they can be embedded in laser systems to provide temperature monitoring of the same point irradiated by the laser. Experiments with temperature control during surgery operations have shown the feasibility of this technology [17–19]. The stability of temperature control can be ±2.5 °C and better. Also, one of the significant advantages of the fiber-optic system is a possible implementation for endoscopic usage. Preliminary experiments with temperature control have already been carried out in urology using an endoscope [20]. The laser system's typical scheme from [9] with continuous temperature control during the operation is presented in Fig. 2. Computer algorithms or a well-known PID system [21] can maintain the temperature during the operation.

The total emissive power collected from a black body and delivered through the PIR fiber has a different temperature dependence than the Stefan-Boltzmann law. The reason is in a non-uniform transmission spectrum of these fibers. After integrating the radiance as described

Biomedical Optics EXPRESS

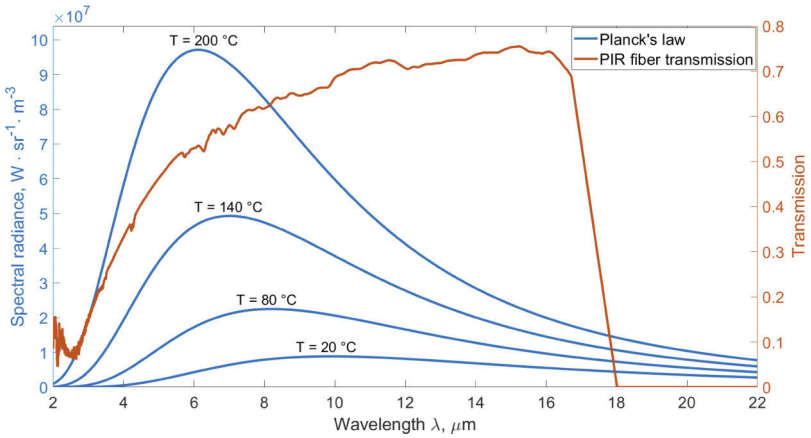

Fig. 1. Planck law, Wien law, and transmission of PIR fiber with 900/1000 μm core/cladding diameters and with 1 m length. Data are available from the company art photonics GmbH [15]. The linear approximation for PIR transmission for wavelengths more than 16 μm was made according to typical PIR transmission [16]

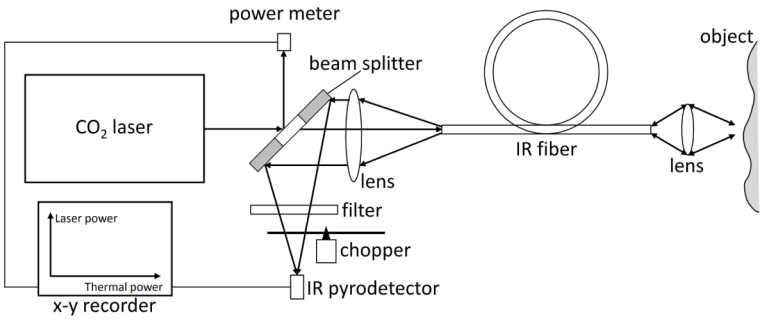

Fig. 2. Typical scheme of a laser system with continuous temperature control during operation, corresponding to [9].

by the Planck law multiplied on a PIR fiber transmission over all wavelengths, we get a modified Stefan-Boltzmann law, which describes the total emissive power delivered from a black body through PIR fiber (see Fig. 3). For temperature range from 20°C to 200°C we can approximate the dependence of the total emitted power j from a black body, delivered through a silver halide fiber, on the temperature T as

$$j \sim T^x, \quad x \approx 4.3, \tag{2}$$

that is close to the Stefan-Boltzmann law.

It is also interesting for practical use to know how much of the thermal energy from a black body will be delivered through PIR fiber to the sensor. Figure 4 shows the temperature dependence for the ratio of radiation power on the black body delivered through the 1 m of PIR fiber to the power radiated directly from the black body, i.e., it shows

$$\frac{\int_0^\infty I(\lambda,T)T_{fiber}(\lambda)d\lambda}{\int_0^\infty I(\lambda,T)d\lambda} = \frac{\int_0^\infty I(\lambda,T)T_{fiber}(\lambda)d\lambda}{\sigma T^4}, \tag{3}$$

where λ is a wavelength of light, $I(\lambda,T)$ is the spectral density of electromagnetic radiation emitted by a black body in thermal equilibrium at a given temperature T (Planck law), T_{fiber} is a transmission of PIR fiber, and σ is the Stefan-Boltzmann constant.

Biomedical Optics EXPRESS

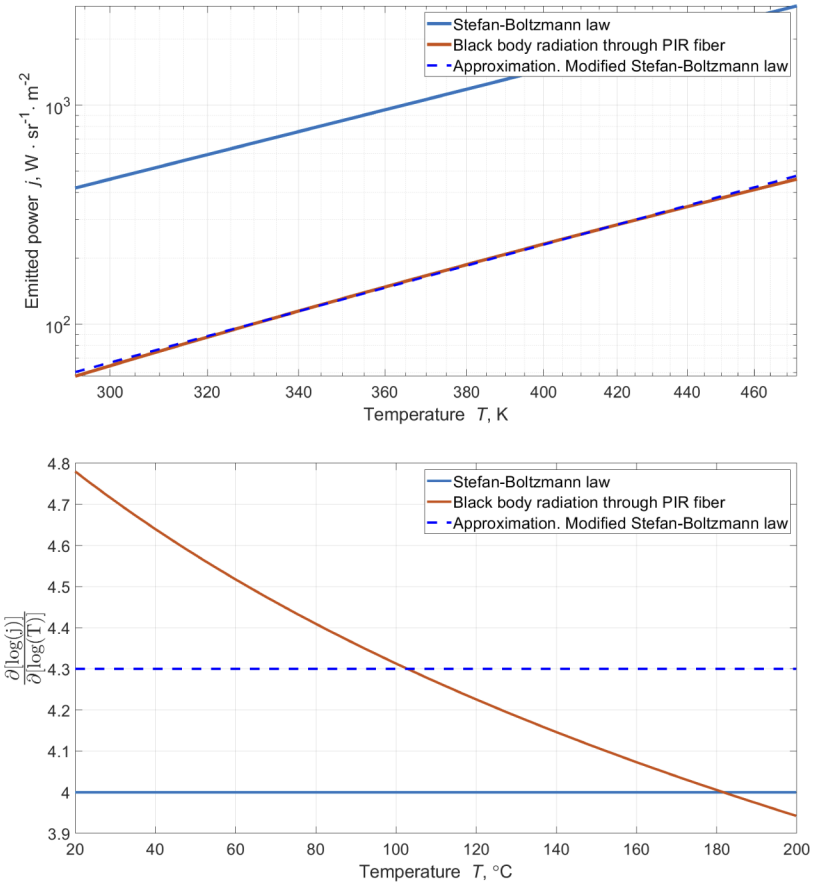

Fig. 3. Comparison of the Stefan-Boltzmann law with total emitted power through the PIR fiber (on top). The slope of the dependence of the emitted power on the logarithm of temperature (on bottom).

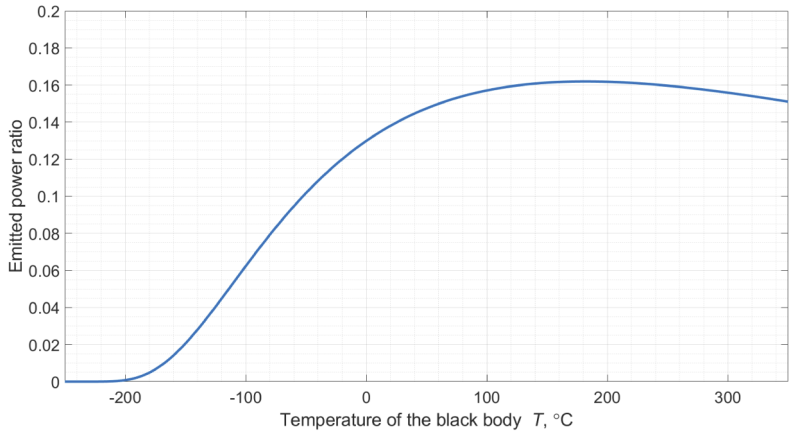

Fig. 4. The ratio of the power delivered through 1 m PIR fiber from the black body to the power from a black body (Planck law), in accordance with Eq. (3).

Biomedical Optics EXPRESS

2. Materials and methods

2.1. Measurement equation

A commercial pyrometer can be used to measure the object's temperature by collecting the IR radiation through the PIR fiber. In common, such pyrometers are usually already calibrated at the factory for the free space measurements. They can show the measured object's actual temperature only if the whole object is located in the pyrometer's detector field of view (FOV). In other words, this device works correctly only in the free space arrangement, and collected IR radiation comes only from the measured object. Therefore, for fiber-optic arrangement, recalibration must be done. One of the simplest methods for it is based on the Stefan-Boltzmann law.

Two coefficients must be introduced to consider all the losses on the optical path and mismatching (when the signal not from the object of interest reaches the detector). The losses due to the atmospheric attenuation are assumed to be zero as a distance where the IR signal is traveling in free space is small enough [22]. The required coefficients are determined by balancing the radiation power $P(T)_{Pyro\ raw}$ at the active surface of the detector:

$$P(T)_{Pyro\ raw} = P(T)_{Detector} + P(T)_{Object} \cdot \varepsilon + P(T)_{Ambient} \cdot (1 - \varepsilon), \tag{4}$$

where $P(T)_{Detector}$ corresponds to the radiant power that comes from the detector environment to the detector's active area (it is the radiation that came not from the object of interest). $P(T)_{Ambient}$ is the radiation power of the ambient temperature coupled into the fiber via reflection from the object. The heat radiation power coupled into the fiber from the object corresponds to $P(T)_{Object}$. Schematically it is shown in Fig. 5.

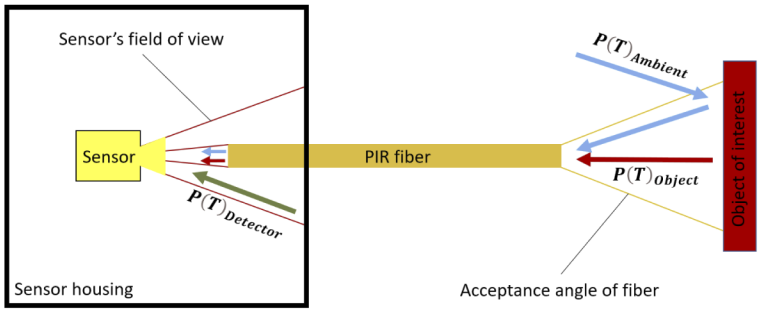

Fig. 5. Scheme of the IR radiation collected by the sensor using PIR fiber.

The following equation results by using a classical Stefan–Boltzmann law and introducing the detector coefficient B describing the amount of power collected not from the target object and the coefficient C describing collected power from the object of interest with the attenuation by the PIR fiber and during the propagation through the optical path:

$$T^4_{Pyro\ raw} = B \cdot T^4_{Detector} + C \cdot (T^4_{Object} \cdot \varepsilon + T^4_{Ambient} \cdot (1 - \varepsilon)). \tag{5}$$

The right part of this equation (multiplied by coefficient C) is similar to the so-called "combined measurement equation" where the Stefan-Boltzmann law was used for the calibration function [23]. With the additional simplification that the ambient temperature is the same for both the detector and a reflection from the object of interest ($T_{Ambient} = T_{Detector}$), the following equation derives:

$$T_{Object} = \left(\frac{T^4_{Pyro\ raw} - T^4_{Ambient} \cdot (B + C - C \cdot \varepsilon)}{C \cdot \varepsilon} \right)^{1/4}. \tag{6}$$

The object temperature can be calculated from the raw data of the detector using Eq. (6). To determine the coefficients B and C, it is enough to make two measurements with two different

Biomedical Optics EXPRESS

temperatures of the heated object and solve the linear system of two equations. Calibration is made when the laser is turned off. The cable's end is placed in front of the heated black metal plate. The plate's temperature is measured using the thermocouple type K. The calibration is made on the temperatures 50° C and 80° C. It was assumed and used the value of emissivity ε=0.95.

2.2. Fiberoptic pyrometer

At first, a compact "Fiber pyrometer" for flexible temperature measurement was constructed. It consists of an IR detector MLX90614 (Melexis Inc., USA) with an FOV of 90° that is based on the principle of a thermopile; microcontroller; and flexible cable with 0.7 m length based on PIR fiber (art photonics GmbH, Germany) with 900/1000 core/clad diameters surrounded by a protective tubing of Polyether ether ketone (PEEK). The heat radiation is detected by the PIR fiber and passed on to the detector. The whole device is placed into small metal housing with protection from humidity. The measurement data can be read using a microcontroller via a mini USB cable and is plotted on the computer. The cable can be easily changed via an SMA connector. The experimentally determined range of vision of the fiber sensor corresponds to an opening angle of about 31° and a numerical aperture of 0.51. The scheme and photo of the device are presented in Fig. 6.

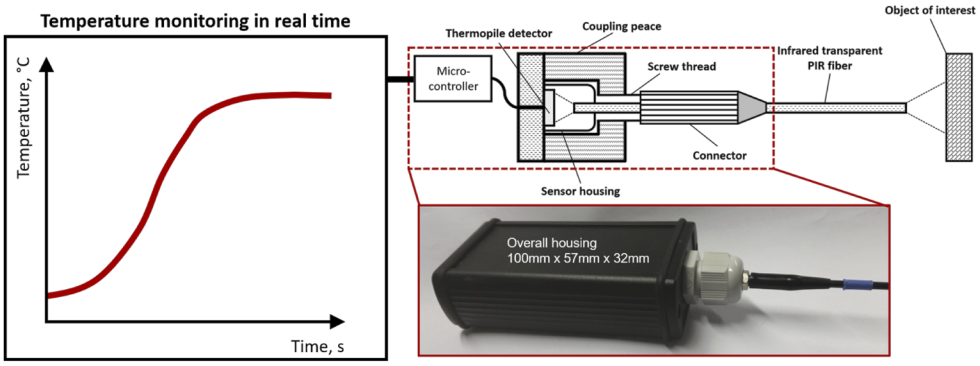

Fig. 6. Fiber pyrometer with an infrared sensor inside and an IR fiber (e.g., PIR fiber) connected to it.

This device is coupled together with a medical laser to provide temperature feedback during surgery. The design of the application part (applicator) consists of an application fiber, which delivers laser radiation, and a sensor fiber, which collects IR radiation from the target point and provides data for temperature calculation. In everyday clinical practice, the application fiber is in contact with the tissue and can "stick" to the surface during application. This effect can be reduced by using the flattest possible angle between the tissue and the application fiber, thus achieving more uniform results during the application. Because of ergonomic considerations during application and the need for good energy input into the tissues, this angle cannot be chosen arbitrarily small, so an angle of approx. 30° was chosen between the tissue and the application fiber.

With an increasing distance of the PIR fiber to the tissue surface, the spatial resolution of the pyrometric sensor deteriorates so that the fiber end should be brought as close as possible to the surface. This distance cannot be chosen arbitrarily small due to the following aspects. Direct temperature transmission through heat conduction and convection to the end of the PIR fiber must be avoided, as this is also measured and leads to incorrect measurements. Furthermore, the fiber end face contamination must be prevented during the application, which can also be a source of error. The opposite is that the area affected by the application fiber becomes smaller compared

Biomedical Optics EXPRESS

to the FOV captured by the sensor as the distance between the sensor fiber and the tissue surface increases. Based on the experiments for the determination of the FOV of the sensor fiber, a measuring spot has a diameter of about 6 mm at a distance of 5 mm from the sensor fiber to the surface. The hotspot caused by the application fiber with its radial temperature outlets, on the other hand, can be estimated with a diameter of 2 mm to 2.5 mm, depending on the laser power. This means that the temperature detected by the sensor fiber is an integration of the temperature in the hotspot and the temperature of the surrounding tissue. A distance of 5 mm between the sensor fiber and the tissue surface protects the fiber end face from contamination, especially if the application fiber is not oriented perpendicular to the tissue surface. The pyrometric fiber sensor detects the maximum signal when placed perpendicularly to the tissue.

Based on these considerations, an applicator design results from a straight guide tube for the application fiber and a double-curved guide tube for the sensor fiber (Fig. 7). Since the sensor fiber is very rigid, sensitive, and comparatively expensive compared to the application fiber, the detector is housed directly in the handle housing. For later commercial use, the end of the guide tube for the sensor fiber can be provided with a protective polyethylene window, which ensures the sterilizability and bio-compatibility of the applicator with good transparency for heat radiation. Figure 7 also shows the first design proposal for a surgical probe prototype with an integrated application and sensor fiber. In the measurements on tissue an infrared camera (Optris PI 640, Germany) is used for a comparative non-contact temperature measurement.

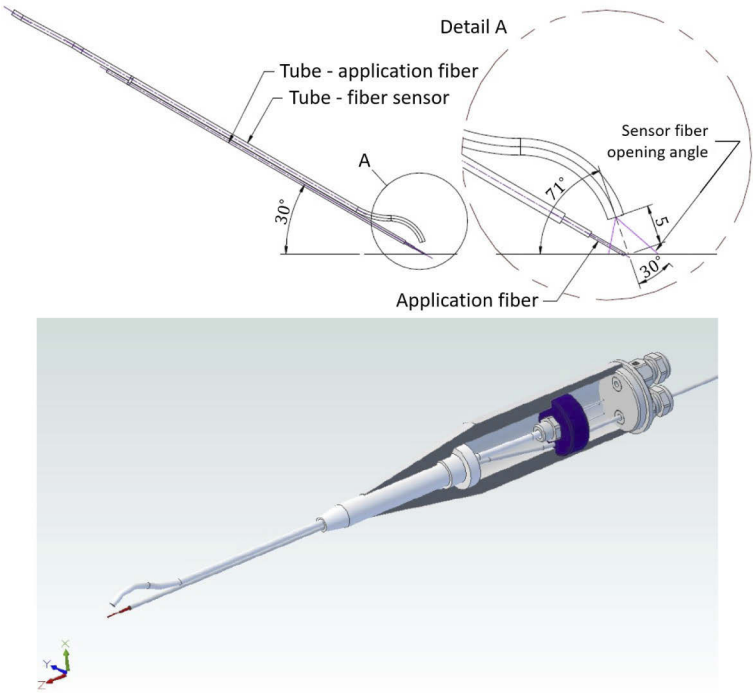

Fig. 7. Technical drawing of the prototype of a combined application and sensor fiber unit (top image). Design proposal for a laser surgical applicator with integrated in-situ temperature control (bottom image).

Biomedical Optics EXPRESS

2.3. Free space system with a single fiber for a laser power delivery and temperature measurement

The scheme of the free space experimental setup with a CO_2 laser with simultaneous temperature control is presented in Fig. 8. In this setup the laser was operated in a pulse regime synchronized with a chopper to avoid the infrared detector damage due to the reflected laser radiation from the PIR fiber end face. Here the chopper was operated at 100 Hz frequency, and for the detector, it effectively served as an additional attenuator of the signal. Experimental setup includes a CO_2-laser source with a maximum 10 W output power (Diamond C-40 air-cooled laser GEM 40A Circular, Coherent Inc., USA) and necessary optical components (from Thorlabs, USA) optimized for the mid-IR region. Reference power meter (Thorlabs, USA) is to calculate transmitted power. Optical chopper (Scitec instruments, UK) is synchronized with laser in such a way that when the chopper is in "closed" position (it doesn't let the radiation to reach the detector) the laser is on and vice versa. The infrared detector MLX90614 (Melexis Inc., USA) with a FOV of 10° is used to measure the temperature from the target object.

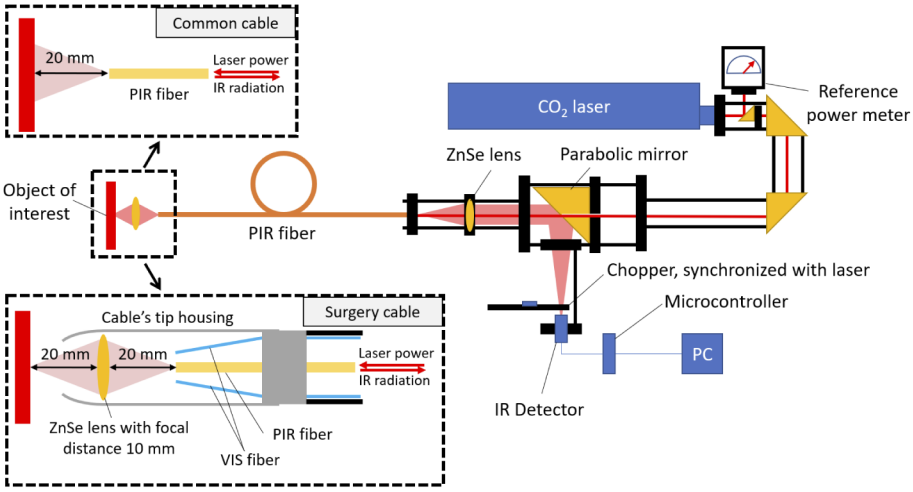

Fig. 8. Optical scheme of the free space experimental setup. Different types of cable are presented. The commercial surgery cable has a mounted lens and 3 fibers inside. PIR fiber is to deliver IR laser radiation and collect IR radiation, and VIS fibers are to provide visible light for focusing on the point (VIS fibers were not used during the experiments).

Two types of cables were used to simultaneously deliver laser power and collect the thermal radiation. The first one is a common PIR cable (art photonics GmbH, Germany) with 900/1000 μm core/clad diameters and 0.7m length surrounded by a protective sleeve of Polyether ether ketone (PEEK). This fiber has about 70% transmission for CO_2 laser radiation (10.6 μm). The second cable is a 1m length commercial surgery cable (MedArt, Denmark) that has a PIR fiber inside with a 600/700 μm core/clad diameters. It has a ZnSe lens with a focal distance of 10 mm and placed on the 20 mm distance from the fiber end. The cable was placed at a 20 mm distance from the object of interest. This cable has about 50% transmission for CO_2 laser radiation (10.6 μm). Microcontroller reads the measurement data and plots it on the computer. The measurement system were tested at the temperatures 60 °C, 90 °C, and 33 °C using the same setup with a heated black metal plate and thermocouple as in the calibration process.

Biomedical Optics EXPRESS

3. Results and discussion

3.1. Calibration, stability, and application of fiber-optic pyrometer

It was found that over time the temperature values shown by the sensor with PIR fiber decreases. After two years in storage it showed the temperature of a human finger as 26 °C. After cutting the PIR fiber end, the sensor showed a temperature of 30 °C. After new calibration the sensor showed the temperature of 32 °C – the same as from the commercial detector. One reason is in the aging mechanism in PIR fiber and on its end faces. The internal structure of the PIR fiber has a crystal nature and during the time a recrystallization occurs leading to a decreased transmission of the fiber [10]. In addition, the fiber end has a constant contact with the environment and may suffer a contamination. The later one can be eliminated by cutting the end, however aging effect due to the internal physical processes will require recalibration or changing the fiber to a new one.

The fundamental suitability of the pyrometric fiber sensor was subsequently tested in various preliminary tests. This included both measurements on artificial objects, such as ovens, hot plates, and first experiments on animal tissue (porcine muscle and liver). Finally, to verify the accuracy of the pyrometric fiber sensor, selective heat sources were generated over a longer period of several seconds using the laser, and the IR camera's measurement signal was compared with that of the fiber sensor (Fig. 9). In this experiment, the diode laser Diolas Photon (Limmer Laser GmbH, Germany) was pulsed with a duty factor of 40% (20 ms on, 30 ms off), so that the cardboard as a sample here does not burn even with prolonged exposure of the laser radiation. The selected laser powers were between 1.3 W and 1.7 W at a wavelength of λ = 980 nm. The end face was positioned at a distance of 1.2 mm from the sample surface to obtain uniform results and avoid the application fiber contamination.

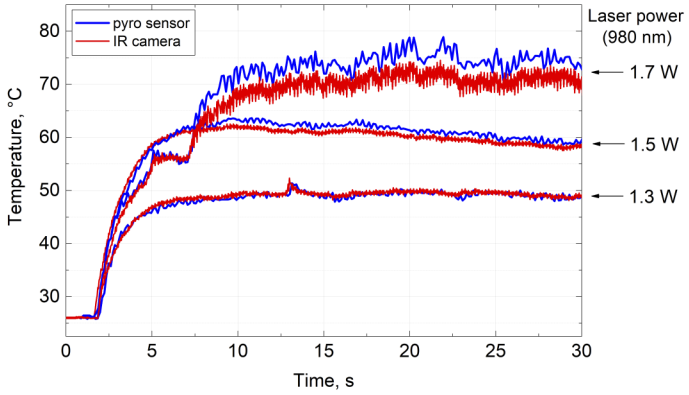

Fig. 9. Measurements of the signal from cardboard as a sample irradiated by a pulsed diode laser. Comparison between the signal measured on the fiber-optic pyrosensor and on the IR camera.

3.2. Fiberoptic pyrometry during tissue treatment with laser

For further testing of the pyrometric fiber sensor and the applicator design, the development of a test setup under realistic test conditions is important. Next experimental setup is used to determine the carbonization limit, with the aim to find an average measured temperature at which no carbonization is currently occurring on the tissue. This measured average temperature is always an "integrated temperature" of the hot spot and ambient temperature due to the larger FOV of the sensor fiber in relation to the area affected by the application fiber. The aim is to be able to derive control of the irradiation result, independent of the preset laser power.

Biomedical Optics EXPRESS

The functional model of the applicator consists of the guide tubes for sensor and application fiber described in the previous chapter (Fig. 7). The guide tubes are connected to each other and rotated at a fixed point. At the front end, the application fiber rests on the tissue, the arrangement is selected so that an angle of 30° is formed between the application fiber and the tissue. At the front one-third of the guide tubes, a small weight is attached, which presses the application fiber with constant force on the tissue and thus creates a uniform contact pressure. The tissue sample lies on a movable sliding table and is moved at a constant speed 2 mm/s under the applicator. Application traces of approximately 30 mm to 40 mm can be achieved depending on tissue sample size. For this application test, the laser system was operated at a wavelength of λ = 1500 nm in continuous mode (CW).

Each experiment was carried out with constant laser power and left a visible line on the tissue – from initial coagulation to strong carbonization. By gradually increasing the laser power, the carbonation limit can be determined visually. In order to have the most uniform test conditions possible, the fiber end of the application fiber is cleaned before each test. The photo of the setup with the applicator is shown in Fig. 10.

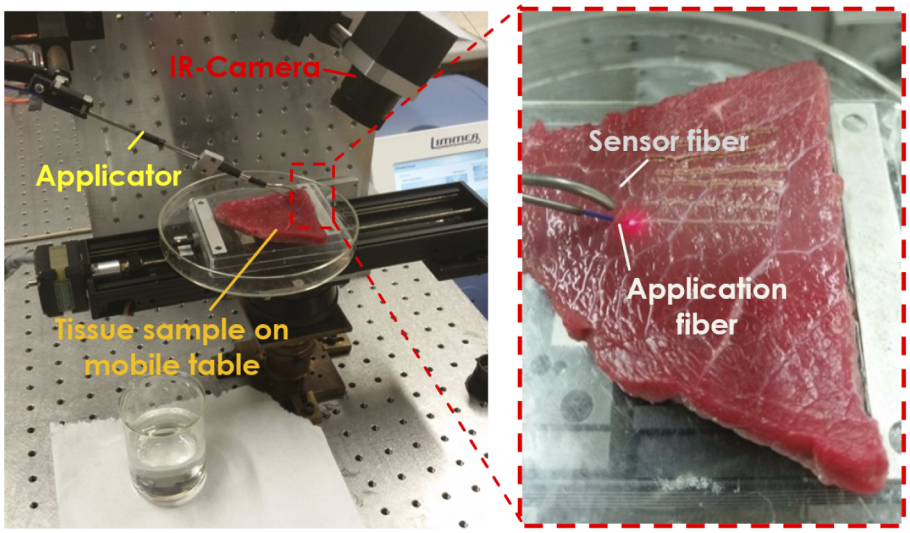

Fig. 10. Experimental setup with the prototype of a combined application and sensor fiber exemplified during use on animal tissue.

Figure 11(a-c) shows the "integrated temperature" recorded by the pyrometric fiber sensor along the application path at different laser powers for different tissue samples (porcine muscle = porcine steak, beef 1 = beef steak, beef 2 = beef roulade). The strong fluctuations in the measured temperature occurred due to the inhomogeneity of the tissue, including the change of emissivity (and thus also change of absorptivity).

After visual comparison with the treated tissue, the measurements are color-coded from green (= no carbonization, only coagulation) to Blue (= beginning carbonization) to Red (= strong carbonization). As an example, in Fig. 11(d-f), microscope images of the tissue samples have been selected on the left side of each page after application, showing the transition between non-carbonized tissue (top) and the beginning of the carbonization (bottom). With the help of IR camera, the spatial temperature distribution at the position and moment of the maximum temperature input along the application path is shown to the right of the microscope image. The temperatures generated in the hotspot can be determined (temperature profiles on the far right in the respective figure), which are directly related to the degree of carbonization.

Biomedical Optics EXPRESS

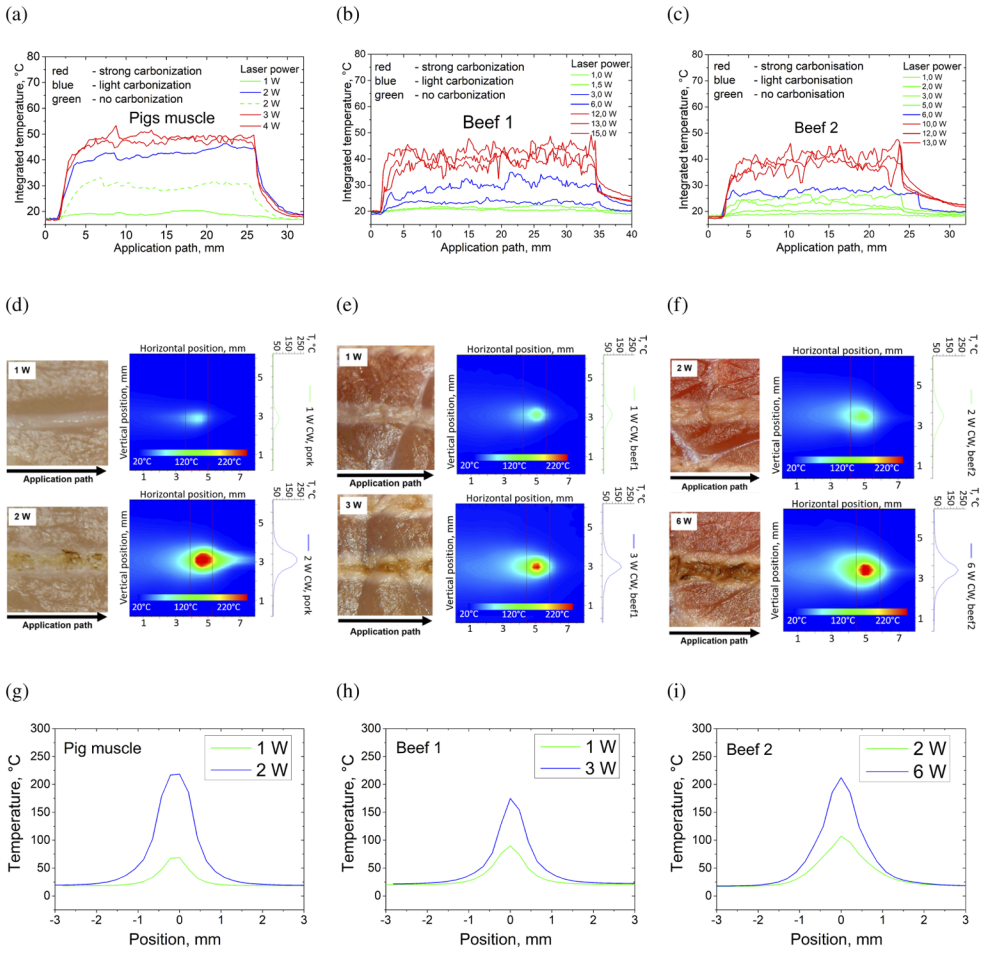

Fig. 11. (a-c) The "integrated temperature" recorded by the pyrometric fiber sensor along the application path at different laser powers for different tissue samples (porcine muscle = porcine steak, beef 1 = beef steak, beef 2 = beef roulade). The applicator was moved at a speed of 2 mm/s relative to the tissue. The application laser was operated at a wavelength of λ = 1500 nm in CW mode. (d-f) On the left, the microscope images of samples after applied laser radiation along the application path. The treated tissue (in d is a porcine muscle, in e is beef steak, in f is beef roulade corresponding to a, b and c) is coagulated (top) or begins to carbonize (bottom). The spatial temperature distribution is shown in the middle. On the right, the temperature profile of the respective hotspot is shown. (g-i) Comparison of the two temperature profiles from (d), (e), and (f) running through the respective hotspot.

Within the FOV of the sensor, not only the temperature at the application site (hotspot) is recorded, but also the temperature of the surrounding tissue (here between 17 °C and 22 °C). Thus, the values recorded by the sensor correspond to an "integrated temperature" of the hotspot and ambient tissue temperature. Depending on how high the temperature input at the application site is, the area contributing to the overall measurement also varies. A rough estimate of this can be derived from the IR images in Fig. 11(d-f). It was noted before that the FOV of the sensor measures approx. 6 mm in diameter on the tissue surface. The surfaces affected by the application fiber have a diameter of 2 mm to 2.5 mm depending on the laser power. The first approximation results in the area ratios between 9:1 ($(6\ \text{mm})^2/(2\ \text{mm})^2$) and 6:1 ($(6\ \text{mm})^2$:(2.5

Biomedical Optics EXPRESS

mm)^2). However, as it can be seen on Fig. 11(d-f), the temperature profiles are not flat-top and have a gaussian-like shape. Thus, the full width at half maximum (FWHM) of these profiles can be used as a size of the area affected by the application fiber. In other words, only part of the FOV detected by the sensor effectively contributes to the increase in temperature. The sensor data must be weighted according to the area ratios if one wants to establish a reference value for the carbonization limit. The weighting can be done using a Stefan-Boltzmann law implemented in the next equation:

$$T^4_{integrate} = f \cdot T^4_{hotspot} + (1 - f) \cdot T^4_{surrounding}\,, \tag{7}$$

where $T_{integrated}$ is the integrated temperature of the hotspot and ambient tissue recorded by the pyrometric fiber sensor, $T_{hotspot}$ is the maximum temperature in the area affected by a laser via application fiber, $T_{surrounding}$ is the constant temperature of the surrounding tissue and $f = S_{hotspot}/S_{FOV}$ is the ratio between the size of the area $S_{hotspot}$ affected by the application fiber and the area S_{FOV} corresponding to the FOV of the sensor fiber. A corresponding overview of the measured integrated temperature, the hotspot temperature recorded by the IR camera, and the temperature ranges specified after the weighting are summarized in Table 1.

Table 1. Overview of measurement results

Tissue type	Carbonization limit from the IR camera, °C	Integrated temperature from the fiber sensor, °C	Temperature of the surrounding tissue, °C	Weighting factor f	Error limits of the fiber sensor, ° C	Applied laser power, W
Porcine muscle	>225[a]	39 - 45	20	0.0261	272 - 312	2
Beef 1	170	23 - 26	22	0.0161	71 - 155	3
Beef 2	210	25 - 30	18	0.0250	162 - 217	6

[a]Due to the lack of spatial resolution of the IR camera, this value is higher than specified

Figure 11(a) shows the measurements with the integrated probe on porcine muscles. The applied laser powers in the porcine muscle were between 1 W and 4 W. The beginning of carbonization was already observed at a power of 2 W and an integrated temperature measured by the fiber sensor from 39 °C to 45 °C. After a corresponding weighting of the measured values, as described above, a limit temperature for the carbonization in the porcine muscle results between 272 °C and 312 °C. Strong carbonization of the tissue occurred from laser lines of 3 W. In Fig. 11(d) the temperature profiles are shown by the respective hotspot, taken with the IR camera. Figure 11(g) compares these two hotspot temperatures. Carbonization thus occurs at 2 W laser power and a corresponding hotspot temperature of 225 °C. Although this value is not within the error interval detected by the fiber sensor, due to the low spatial resolution and saturation of the IR camera at a maximum temperature of 279 °C per pixel, a "virtual" plateau formation can be observed (Fig. 11(g)). It can be assumed that the maximum values here are higher and correspondingly within the error intervals.

In addition, a special feature could be observed in the porcine muscle, which directly demonstrates the potential of in-situ temperature measurement. If one compares the carbonization result with a preset laser power of 2 W, both no and incipient carbonization were observed in two different measurements (green dashed and blue curve in Fig. 11(a)). Under certain conditions, such as moisture of the surface, the water content of the cells, the distance of the application fiber to the tissue or tissue, contact pressure, and the "sticking" of the application fiber at a certain point, the result may vary. However, all these conditions are difficult to control, predict and differ from tissue to tissue in clinical use. While the preset laser power provides different results, the in-situ temperature measurement can be used to make a statement about the actual condition of the treated tissue and the laser power can be adapted to the current conditions via corresponding feedback control.

Biomedical Optics EXPRESS

The second type of tissue (beef 1) is beef steak/muscle. Here, laser powers between 1 W and 15 W were applied. Incipient carbonization from a laser power of 3 W was observed. The integrated temperature measured by the sensor fiber was between 23 °C and 26 °C. After weighting, a tolerance interval for the measurements in beef 1 was obtained between 71 °C and 155 °C. The comparison with the IR camera measurements from Figs. 11(e) and 11(h) shows a limit temperature to the carbonization of 170 °C which is close to the limit temperature for carbonization of 155 °C obtained from the fiber sensor in this case.

The third type of tissue is beef Roulade (Beef 2). The applied laser powers are between 1 W and 13 W (Fig. 11(c)). Incipient carbonization was observed at a laser power of 6 W. The integrated temperature recorded by the pyrometric sensor was between 25 °C and 30 °C. After the weighting, a tolerance interval for the limit temperature for carbonization between 162 °C and 217 °C was obtained for the measurements in Beef 2. The temperature profiles extracted from Fig. 11(f) (shown separately in Fig. 11(i)) show a limit temperature to the carbonization of 210 °C. This value is well within the error tolerance of the pyrometric sensor.

An overview of the measurement results is shown in Table 1. The three tissue types have different carbonization limits. It is crucial that the temperature directly recorded by the IR camera, from which carbonization of the tissue can be observed, can also be measured by the pyrometric fiber sensor after weighting the sensor data within the error tolerances.

In this paper, a visual control was used to detect an incipient carbonization. To our knowledge, there is no "gold standard" to define carbonization. During laser surgeries in clinical everyday practice, tissue carbonization as a sign of heat generation is usually evaluated by visual inspection, if possible by magnified imaging using microscopes or endoscopes. Strong carbonization should always be avoided by using appropriate laser parameters in order not to delay tissue healing and to reduce the risk of infection. However, for more precise determination, histological methods can be used for an investigation of carbonization on a microscopic level, e.g. [24,25]. Another potential tool for detection of carbonization could be the Laser-induced breakdown spectroscopy (LIBS). However, this technique seems to be restricted to bone ablation under ex vivo conditions by monitoring the plasma plumes occurring during laserosteotomy procedures. According to the literature, successful differentiation of carbonated and non-carbonated bone results from the intensity ratio of sodium and calcium [26]. Further research is needed to confirm the potential of LIBS and other techniques for in vivo detection of carbonization and clinical applications in other tissue types.

In the experimental setup the size of the laser heating spot is different from that of the measuring hotspot. Therefore, the temperature of the heating spot need to be deduced from the integrated temperature by Eq. (7), which will bring great uncertainty to the measurements. A better solution might be in using a hollow waveguide instead of AgClBr fiber for temperature sensing. It has much lower numerical aperture (NA≈0.05 for a hollow waveguide, NA≈0.3 for AgClBr PIR fiber) and also a broad transmission range. One significant drawback of using a hollow waveguide is that it is much more sensitive to the bending. To overcome this, a combination of the fibers can be used: hollow waveguide in a fixed position mounted in a handpiece and coupled with a AgClBr fiber that comes out from a handpiece and goes to the detector. Such a solution could help to decrease an uncertainty to the measurements and will not make it too complex.

3.3. *Application of the free space system with a single fiber for a laser power delivery and temperature measurement*

For the experiment with a free space system laser with simultaneous temperature control, ordinary porcine meat with a small amount of fat and porcine skin was utilized. It was cut into small pieces (around 50 mm x 50 mm x 20 mm) with a flat top surface. The measurement deviation and noisiness of the system for the PIR cable (0.7 m length) and "surgical" cable (about 1.5 m length) were measured using a heated black metal plate (laser was off). The results are presented

Biomedical Optics EXPRESS

in Table 2. Note that calibration is done on temperatures 50 °C and 80 °C, so the measurement deviation is around zero for these temperatures.

Table 2. Measurement deviation for the free space setup (laser is off). Common cable has 0.7m length 900/1000 μm core/clad diameters PIR fiber inside and 70% CO_2 laser transmission. Surgical cable with lens has 1m length 600/700 μm core/clad diameters PIR fiber inside and 50% CO_2 laser transmission.

Type of cable	Real temperature, °C	Measured temperature, °C	Measurement deviation, °C
Common cable without lens	33 (hand)	30	−3
	60.2	61.2	+1
	92.3	94	1.7
Surgery cable with lens	33 (hand)	32	−1
	59.8	60	0.2
	95.3	95	−0.3

Results with less noise were obtained for the common PIR cable in comparison to a surgical cable with the lens inside. The possible reason is that the transmission for surgical cable was lower, and relatively more radiation from ambient was collected (this also can explain a bigger measurement deviation). Accuracy was a little better (i.e. with less measurement deviation) for a surgical cable with the lens inside that collects a signal from a point. In addition, in real surgical system lens is also can be used to adjust the delivered intensity of light by changing the position of the lens. The precision of 2-3 °C for thermometry in the case of ablative treatments is often acceptable [27].

Then the test on the porcine meat and skin was done with the "surgical cable" that was placed at a distance of 20 mm from the object. Samples were irradiated by different CO_2 laser powers. During the test on porcine's meat the mount was manually moved with constant speed using micrometer screws to maintain the temperature. The 2 lines with ablation were obtained while the 3 lines were exposed (Fig. 12). The third line did not show any changes in color underexposure. For the bottom line, the measured temperature was about 45 °C, and there was no coagulation of the proteins: the color was not changed. For the left line we can clearly see the carbonization in the points (the color changed to brown and black) when the mount was stopped and the laser-induced temperature raised to critical points. A wider ablated area was observed for the left line comparing. In addition, the test on paper was conducted: the laser power was increased and the paper was burned when the measured temperature rises to around 220°C, that is in a good agreement with the autoignition temperature of paper of 232°C [28]. Then the temperature drops down as a hole appeared.

In the simple recalibration procedure used in the experiments, only two temperature points were used. To improve an accuracy of the system more temperature points for calibration must be used. Another way for calibration is to measure the power of the IR signal from the target object and build the dependence with a real temperature of this object. However, after some time, as discussed above, because of the aging effects in fiber, or changing optics in a setup, the recalibration must be done. In addition, it is essential to use a proper optics on the optical path from the irradiated sample to the detector because optical elements also absorb the light and can be heated at high laser power that will give an addition signal to the detector.

Another thing to note is that fibers were fixed during the measurements. It is known that during the bending of the fiber, so-called bending losses take place, and fiber transmission decreases. However, optical properties of the silver halide polycrystalline fibers used in the experiment are tolerant to the normal bending [10] (in our case a bending diameter is more than 40 cm). Thus, it is expected that the bending effect on the system performance will be negligible.

Biomedical Optics EXPRESS

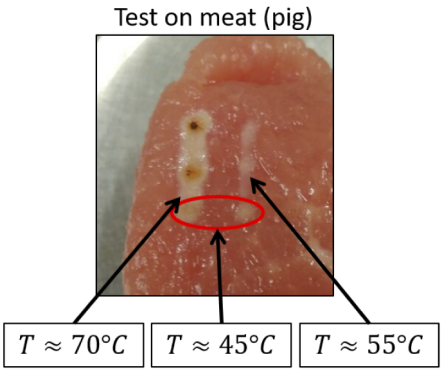

Fig. 12. Meat's surface where CO_2 laser radiation were applied along 3 lines. The measured temperature for each line during the moving of the mount with cable is shown. Temperature measurement and laser exposure were done simultaneously.

4. Conclusion

A novel surgical probe consisting of an application fiber for delivery of laser radiation and a sensor fiber for in-situ temperature control was developed, various temperature measurements were carried out on tissue samples, and a prototype was created. The data collected by the sensor fiber can be transmitted to an electronic feedback unit and used to control the applied laser power. Quantitative characterization of the pyrometric sensor alone and combined with an application fiber for surgical laser radiation has been performed. The stand-alone temperature module was demonstrated for a temperature range between 20 °C and 300 °C.

In order to demonstrate the simultaneous use of a single PIR fiber for temperature control in combination with laser beam guiding for treatment of tissue samples, the criterion of "incipient carbonization" of tissue was introduced. With the built-up system, it was possible to determine whether a current laser power leads to a carbonization. Complex boundary conditions, which can also be found in clinical use, could be taken into account (degree of moisture and unevenness of the tissue as well as the type of tissue). Different tissue types, for example, lead to different results at the limit temperature that must be defined before carbonization can occur. This can be taken into account by creating a tissue database. For each of the tissue types investigated here (pig muscle, cattle 1 and cattle 2), a temperature interval could be specified at which the criterion of incipient carbonization was met. The prototype resulted in a good agreement with a comparison measurement recorded using an IR camera.

By systematic examination of further clinically relevant tissue samples, comparatively wide temperature intervals can be narrowed and specified. For this purpose, the geometry of an applicator consisting of application and sensor fiber constructed for a specific clinical indication must be considered with regard to the resulting FOV of the pyrometric sensor and calibrated once. Subsequently, limit values for the integrated temperature (hotspot + temperature of the surrounding tissue) detected by the pyrometric temperature sensor can be defined, which prevent carbonization of the treated tissue. Short-term exceeding of these limits can be controlled via feedback control system which adjusts the laser power and thus reduces the temperature in the application site, enabling the effect-controlled application of surgical laser.

In summary, the ability to use silver halide polycrystalline fibers in real-time temperature measuring devices was discussed, and a simple recalibration and measurement process was established. In such a device, the laser power can be delivered through the same fiber that collects the infrared thermal radiation from the target surface. The precision and accuracy can be significantly improved by matching the optics, so the detector collects less unnecessary radiation

Biomedical Optics EXPRESS

from "outside". PIR fiber properties such as non-toxicity, biocompatibility and flexibility make them a perfect choice for laser surgery applications with the real-time temperature measurement during the laser exposure that adds more control and possibility for adjustments during the operation. In addition, such fibers can be easily replaced by new ones if required: the fiber applicator can be disposable.

Funding. AIF Projekt GmbH Berlin within the framework of the ZIM program of the Bundesministerium für Wirtschaft und Energie.

Acknowledgments. We acknowledge the work of Christian Nitschke, who made a valuable contribution to the project but passed away.

Disclosures. The authors declare no conflicts of interest.

Data availability. Data underlying the results presented in this paper are available from the authors upon reasonable request.

References

1. B. Jones, "A reappraisal of the use of infrared thermal image analysis in medicine," IEEE Trans. Med. Imaging **17**(6), 1019–1027 (1998).
2. J. Steketee, "Spectral emissivity of skin and pericardium," Phys. Med. Biol. **18**(5), 686–694 (1973).
3. G. J. Tattersall, "Infrared thermography: a non-invasive window into thermal physiology," Comp. Biochem. Physiol., Part A: Mol. Integr. Physiol. **202**, 78–98 (2016). Ecophysiology methods: refining the old, validating the new and developing for the future.
4. X. Geng, Z. Zhou, Q. Li, S. Wu, C.-Y. Wang, H.-L. Liu, C.-C. Chuang, and P.-H. Tsui, "Comparison of ultrasound temperature imaging with infrared thermometry during radio frequency ablation," Jpn. J. Appl. Phys. **53**(4), 047001 (2014).
5. Y. Zhou, "Noninvasive thermometry in high-intensity focused ultrasound ablation," Ultrasound quarterly **33**(4), 253–260 (2017).
6. D. Perpetuini, C. Filippini, D. Cardone, and A. Merla, "An overview of thermal infrared imaging-based screenings during pandemic emergencies," Int. J. Environ. Res. Public Health **18**(6), 3286 (2021).
7. B. Lahiri, S. Bagavathiappan, T. Jayakumar, and J. Philip, "Medical applications of infrared thermography: a review," Infrared Phys. Technol. **55**(4), 221–235 (2012).
8. D. Simhon, I. Gabay, G. Shpolyansky, T. Vasilyev, I. Nur, R. Meidler, O. A. Hatoum, A. Katzir, M. Hashmonai, and D. Kopelman, "Temperature-controlled laser-soldering system and its clinical application for bonding skin incisions," J. Biomed. Opt. **20**(12), 128002 (2015).
9. V. Artjushenko, V. Voitsekhovsky, V. Masychev, J. Zubov, and V. Sysoev, "Fibre optic device for simultaneous laser power transmission and temperature measuring of irradiated object," Electron. Lett. **20**(23), 983–984 (1984).
10. J. A. Harrington, *Infrared Fibers and their Applications* (SPIE-International Society for Optical Engineering, 2003).
11. M. Dirnwöber, "Characterization of optical fibers in the mid-infrared," Diplomarbeit, TU Wien (2005).
12. S. Vilches, Ç. Ataman, and H. Zappe, "Endoscopic pyrometric temperature sensor," Opt. Lett. **45**(7), 1730–1733 (2020).
13. A. Zur and A. Katzir, "Use of infrared fibers for low-temperature radiometric measurements," Appl. Phys. Lett. **48**(7), 499–500 (1986).
14. S. Shalem and A. Katzir, "Silver halide infrared transmitting core/clad fibers with small cores," in *Optical Fibers and Sensors for Medical Applications IV*, vol. 5317 I. Gannot, ed., International Society for Optics and Photonics (SPIE, 2004), pp. 13–21.
15. art photonics GmbH, "Polycrystalline IR-Fibers," https://www.artphotonics.com/product/polycrystalline-ir-fibers. Accessed: 2020-10-30.
16. V. Artiouchenko, V. A. Lobachev, M. Nikitin, T. Sakharova, V. Sakharov, and C. Wojciechowski, "PIR fiber sensing in 4- to 18-um range for flexible IR imaging and process IR spectroscopy," in *Second European Workshop on Optical Fibre Sensors*, vol. 5502 J. M. Lopez-Higuera and B. Culshaw, eds., International Society for Optics and Photonics (SPIE, 2004), pp. 295–299.
17. I. Gabay, I. Barequet, D. Varssano, M. Rosner, and A. Katzir, "Bonding surgical incisions using a temperature-controlled laser system based on a single infrared fiber," J. Biomed. Opt. **18**(11), 111416 (2013).
18. A. Barak, O. Eyal, M. Rosner, E. Belotserkousky, A. Solomon, M. Belkin, and A. Katzir, "Temperature-controlled co2 laser tissue welding of ocular tissues," Surv. Ophthalmol. **42**, S77–S81 (1997).
19. O. Shenfeld, E. Ophir, B. Goldwasser, and A. Katzir, "Silver halide fiber optic radiometric temperature measurement and control of co2 laser-irradiated tissues and application to tissue welding," Lasers Surg. Med. **14**(4), 323–328 (1994).
20. D. Shumalinsky, L. Lobik, S. Cytron, M. Halpern, T. Vasilyev, A. Ravid, and A. Katzir, "Laparoscopic laser soldering for repair of ureteropelvic junction obstruction in the porcine model," J. Endourol. **18**(2), 177–181 (2004). PMID: 15072627.

Biomedical Optics EXPRESS

21. K. H. Ang, G. Chong, and Y. Li, "Pid control system analysis, design, and technology," IEEE Trans. Contr. Syst. Technol. **13**(4), 559–576 (2005).
22. R. Usamentiaga, P. Venegas, J. Guerediaga, L. Vega, J. Molleda, and F. Bulnes, "Infrared thermography for temperature measurement and non-destructive testing," Sensors **14**(7), 12305–12348 (2014).
23. B. Lane, E. Whitenton, V. Madhavan, and A. Donmez, "Uncertainty of temperature measurements by infrared thermography for metal cutting applications," Metrologia **50**(6), 637–653 (2013).
24. K. Matsumoto, H. Suzuki, Y. Usami, M. Hattori, and T. Komori, "Histological evaluation of artifacts in tongue tissue produced by the co2 laser and the electrotome," Photomed. Laser Surg. **26**(6), 573–577 (2008). PMID: 19025408.
25. I. Cercadillo-Ibarguren, A. J. Espa na Tost, J. Arnabat Domínguez, E. Valmaseda Castellón, L. Berini Aytés, and C. Gay Escoda, "Histologic evaluation of thermal damage produced on soft tissues by co2, er, cr:ysgg and diode lasers," Med. Oral. **15**(6), e912–e918 (2010).
26. H. Abbasi, G. Rauter, R. Guzman, P. C. Cattin, and A. Zam, "Laser-induced breakdown spectroscopy as a potential tool for autocarbonization detection in laserosteotomy," J. Biomed. Opt. **23**(7), 071206 (2018).
27. M. A. Lewis, R. M. Staruch, and R. Chopra, "Thermometry and ablation monitoring with ultrasound," Int. J. Hyperthermia **31**(2), 163–181 (2015).
28. S. McAllister, J.-Y. Chen, and A. C. Fernandez-Pello, *Fundamentals of Combustion Processes*, vol. 302 (Springer, 2011).